IKKα controls ATG16L1 degradation to prevent ER stress during inflammation

Michaela A. Diamanti,[1]* Jalaj Gupta,[1]* Moritz Bennecke,[2] Tiago De Oliveira,[1] Mallika Ramakrishnan,[1] Anne K. Braczynski,[3] Benjamin Richter,[4] Petra Beli,[5] Yinling Hu,[6] Maya Saleh,[7] Michel Mittelbronn,[3] Ivan Dikic,[4] and Florian R. Greten[1]

[1]Institute for Tumor Biology and Experimental Therapy, Georg-Speyer-Haus, 60596 Frankfurt am Main, Germany
[2]Institute of Molecular Immunology, Klinikum rechts der Isar, Technische Universität München, 81675 Munich, Germany
[3]Edinger Institute (Institute of Neurology), Goethe University Hospital and [4]Institute of Biochemistry II, Buchmann Institute for Molecular Life Sciences, Goethe University School of Medicine, Goethe University, 60323 Frankfurt, Germany
[5]Institute of Molecular Biology, 55128 Mainz, Germany
[6]Cancer and Inflammation Program, Center for Cancer Research, National Cancer Institute, Frederick, MD 21702
[7]Department of Biochemistry, McGill University, Montreal, Quebec H3G 1Y6, Canada

Inhibition of the IκB kinase complex (IKK) has been implicated in the therapy of several chronic inflammatory diseases including inflammatory bowel diseases. In this study, using mice with an inactivatable IKKα kinase (*Ikkα*$^{AA/AA}$), we show that loss of IKKα function markedly impairs epithelial regeneration in a model of acute colitis. Mechanistically, this is caused by compromised secretion of cytoprotective IL-18 from IKKα-mutant intestinal epithelial cells because of elevated caspase 12 activation during an enhanced unfolded protein response (UPR). Induction of the UPR is linked to decreased ATG16L1 stabilization in *Ikkα*$^{AA/AA}$ mice. We demonstrate that both TNF-R and nucleotide-binding oligomerization domain stimulation promote ATG16L1 stabilization via IKKα-dependent phosphorylation of ATG16L1 at Ser278. Thus, we propose IKKα as a central mediator sensing both cytokine and microbial stimulation to suppress endoplasmic reticulum stress, thereby assuring antiinflammatory function during acute intestinal inflammation.

INTRODUCTION

Inflammatory bowel diseases (IBDs) including Crohn's disease (CD) and ulcerative colitis are characterized by chronic, progressive, and relapsing inflammatory disorders mainly in the large bowel. Genetic, environmental, and intestinal microbial factors seem to be important contributors in the etiology and pathogenesis of IBD (Schirbel and Fiocchi, 2010). Many genetic variants have been identified as CD susceptibility factors. The nucleotide-binding oligomerization domain–containing protein 2 (*NOD2*), which is an intracellular sensor of pathogen-associated molecular pattern, was the first gene to be associated with CD susceptibility (Hugot et al., 2001; Ogura et al., 2001). More recently, a coding polymorphism (Thr300Ala) in *ATG16L1* (autophagy-related 16-like 1) has been identified that confers increased risk for the development of CD (Hampe et al., 2007; Rioux et al., 2007) and significantly increases caspase-mediated cleavage of Atg16L1, resulting in lower levels of full-length Atg16L1(T300A) protein (Murthy et al., 2014). Patients carrying homozygous *ATG16L1* risk alleles and mice with hypomorphic expression of ATG16L1 are both associated with Paneth cell and goblet cell abnormalities (Cadwell et al., 2008; Lassen et al., 2014). Several studies have shown that intracellular sensor NOD1 and NOD2 can play a critical role in the induction of autophagy during bacterial infection. NOD1 and NOD2 recruit ATG16L1 to the plasma membrane at the bacterial entry site (Travassos et al., 2010). These studies highlight the role of autophagy in IBD. In addition to autophagy, ER stress is also associated with the development of IBD. Deletion of *Xbp1* (X box–binding protein 1), a key transcription factor that mediates ER stress, results in spontaneous enteritis and increased susceptibility to experimental colitis (Kaser et al., 2008). Interestingly, ER stress and autophagy are interconnected at many levels (Hotamisligil, 2010). In particular, impaired ATG16L1 function was linked to an enhanced ER stress response (Adolph et al., 2013).

NF-κB is a key regulator of inflammatory response that can be activated by canonical and alternative pathways. The activation of the NF-κB pathway is governed by upstream IκB kinase complex (IKK), which consists of IKKα and/or IKKβ catalytic units and a regulatory scaffold protein NF-κB

*M.A. Diamanti and J. Gupta contributed equally to this paper.

Correspondence to Florian R. Greten: greten@gsh.uni-frankfurt.de

Abbreviations used: CD, Crohn's disease; DSS, dextran sodium sulfate; DTT, dithiothreitol; GST, glutathione S-transferase; H&E, hematoxylin and eosin; IBD, inflammatory bowel disease; IEC, intestinal epithelial cell; IKK, IκB kinase complex; MDP, muramyldipeptide; NEMO, NF-κB essential modulator; NOD, nucleotide-binding oligomerization domain; qRT-PCR, quantitative RT-PCR; UPR, unfolded protein response; XBP1, X box–binding protein 1.

The Rockefeller University Press $30.00
J. Exp. Med. 2017 Vol. 214 No. 2 423–437
https://doi.org/10.1084/jem.20161867

essential modulator (NEMO)/IKKγ (Bollrath and Greten, 2009). During canonical NF-κB activation, inhibitory IκBα is primarily phosphorylated by IKKβ, which leads to its proteasomal degradation, whereas IKKα controls the alternative activation of NF-κB by phosphorylation of NF-κB2/p100, which leads to processing and liberation of p52/RelB active heterodimer (Häcker and Karin, 2006). Several mouse studies have revealed tissue- and context-dependent functions of canonical NF-κB signaling in various models of colitis. For example, local administration of NF-κB p65 antisense oligonucleotide abrogates both chemically induced colitis and colitis observed in *Il10* knockout mice (Neurath et al., 1996). Deficiency of IKKβ in myeloid cells but not in intestinal epithelial cells (IECs) ameliorates chronic colitis of *Il10* knockout mice; however, IEC-specific deletion of *Ikkβ* or pharmacological inhibition of IKKβ results in exacerbated acute colitis induced by dextran sodium sulfate (DSS) administration (Greten et al., 2004; Eckmann et al., 2008). Additionally, NEMO/IKKγ-dependent NF-κB activation is indispensable for intestinal homeostasis, as specific deletion of *NEMO/Ikkγ* causes spontaneous intestinal inflammation and colitis (Nenci et al., 2007). Moreover, IEC-specific *Ikkβ* deletion results in exacerbated pathogen-specific IFN-γ and IL-17 responses and severe intestinal inflammation after infection with parasite *Trichuris* (Zaph et al., 2007). Recently, it has been shown that IEC-specific IKKα, but not IKKβ, is critical to control intestinal inflammation and bacterial dissemination to peripheral organs upon *Citrobacter rodentium* infection, thus linking alternative NF-κB activation to antibacterial immunity (Giacomin et al., 2015). However, little is known about the role of IKKα in the pathogenesis of IBD.

Here, we examined the function of IKKα in a model of DSS-induced colitis and identify a complex intracellular signaling network linking TNF-R– and NOD-dependent IKKα kinase activity to stabilize ATG16L1 thereby governing ER stress and subsequent activation of caspase 12, which is ultimately involved in IL-18 processing and epithelial regeneration.

RESULTS

IKKα in IECs protects from DSS-induced colitis

To examine the function of IKKα during acute colitis, $Ikk\alpha^{AA/AA}$ knock-in mice were orally challenged with DSS in drinking water for 5 d followed by 4 d of regular water during recovery (Kitajima et al., 1999). $Ikk\alpha^{AA/AA}$ mutants that lacked inducible kinase activity (Cao et al., 2001) revealed increased susceptibility to DSS, which was characterized by significantly increased weight loss, a higher histological damage score, and elevated number of ulcerations compared with *Wt* mice (Fig. 1. A–E; and Fig. S1 A). This was paralleled by marked up-regulation of genes coding for proinflammatory cytokines and chemokines including IL-1β, TNFα, IL-6, CXCL1, CXCL2, and CCL2 as well as enhanced cyclooxygenase 2 (COX-2) and matrix metalloproteinase 9 (MMP-9) expression in whole colonic mucosa from DSS-challenged $Ikk\alpha^{AA/AA}$ mice (Fig. 1, F and G). To determine whether IKKα functions in IECs or hematopoietic cells to control DSS-induced tissue damage, we performed adoptive transfer experiments. $Ikk\alpha^{AA/AA}$ mutants receiving either $Ikk\alpha^{Wt/Wt}$ or $Ikk\alpha^{AA/AA}$ bone marrow continued to develop more severe colitis, whereas transfer of $Ikk\alpha^{AA/AA}$ bone marrow cells into $Ikk\alpha^{Wt/Wt}$ recipients slightly improved DSS-induced damage (Fig. 1, H and I), indicating that IKKα activation in IECs was mainly responsible for providing protection from DSS-triggered inflammation. This was further confirmed using animals with cell type–restricted *Ikkα* deletion. Mice lacking *Ikkα* specifically in IECs ($Ikk\alpha^{\Delta IEC}$) developed significantly more severe colitis, whereas loss of IKKα in myeloid cells ($Ikk\alpha^{\Delta mye}$) improved disease outcome (Fig. 1, J–M; and Fig. S1 B). To address whether the alternative NF-κB activation pathway (Senftleben et al., 2001) was responsible for the effects mediated by IKKα, *Nfkb2*-deficient mice were challenged with DSS. However, loss of NF-κB2/p100 did not aggravate DSS-triggered inflammation (Fig. 1, N and O). Collectively, these data indicated that independently of the alternative NF-κB pathway, IKKα-mediated signaling in IECs is essential to suppress excessive inflammatory responses and, thus, maintaining intestinal tissue integrity during DSS-induced acute colitis.

Loss of IKKα function triggers an IRE1α–dependent unfolded protein response (UPR) and caspase 12 activation

When we examined expression of various genes associated with cellular stress response that could explain the increased susceptibility of $Ikk\alpha^{AA/AA}$ mice to DSS, we found elevated levels of *Ire1a* and *Ire1b* in unchallenged $Ikk\alpha^{AA/AA}$ IECs (Fig. 2 A). Indeed, ER stress has been associated with development of IBD (Kaser et al., 2008), and recently loss of IKKα function has been linked to enhanced ER stress in a model of acute pancreatitis (Li et al., 2013). Moreover, DSS administration led to substantial Grp78 up-regulation in *Ikkα* mutants (Fig. 2 B). In contrast, phosphorylation of protein kinase RNA-like ER kinase (PERK) and induction of CCAAT/enhancer-binding protein homologous protein (Chop) expression was markedly enhanced in $Ikk\alpha^{Wt/Wt}$ IECs, yet absent in $Ikk\alpha^{AA/AA}$ IECs (Fig. 2 C). Phosphorylation of eIF2a was indifferent between the two genotypes (Fig. 2 C) indicating a specific activation of the IRE1α-dependent UPR signaling cascade in $Ikk\alpha^{AA/AA}$ IECs upon DSS exposure. ER stress–induced IRE1α overexpression and subsequent transautophosphorylation activates its RNase activity to initiate nonconventional splicing of XBP1 mRNA (Calfon et al., 2002). Consistently, DSS induced enhanced XBP1 splicing in DSS-challenged $Ikk\alpha^{AA/AA}$ IECs compared with $Ikk\alpha^{Wt/Wt}$ IECs (Fig. 2, D and E). Furthermore, in agreement with elevated ER stress and IRE1α up-regulation, TRAF2 was degraded (Fig. 2 F), which has been suggested to be involved in IRE1α-dependent caspase 12 activation (Yoneda et al., 2001; Hu et al., 2006). Indeed, cleaved caspase 12 expression was also markedly enhanced in $Ikk\alpha^{AA/AA}$ IECs during DSS administration (Fig. 2 G). To confirm that elevated ER stress in

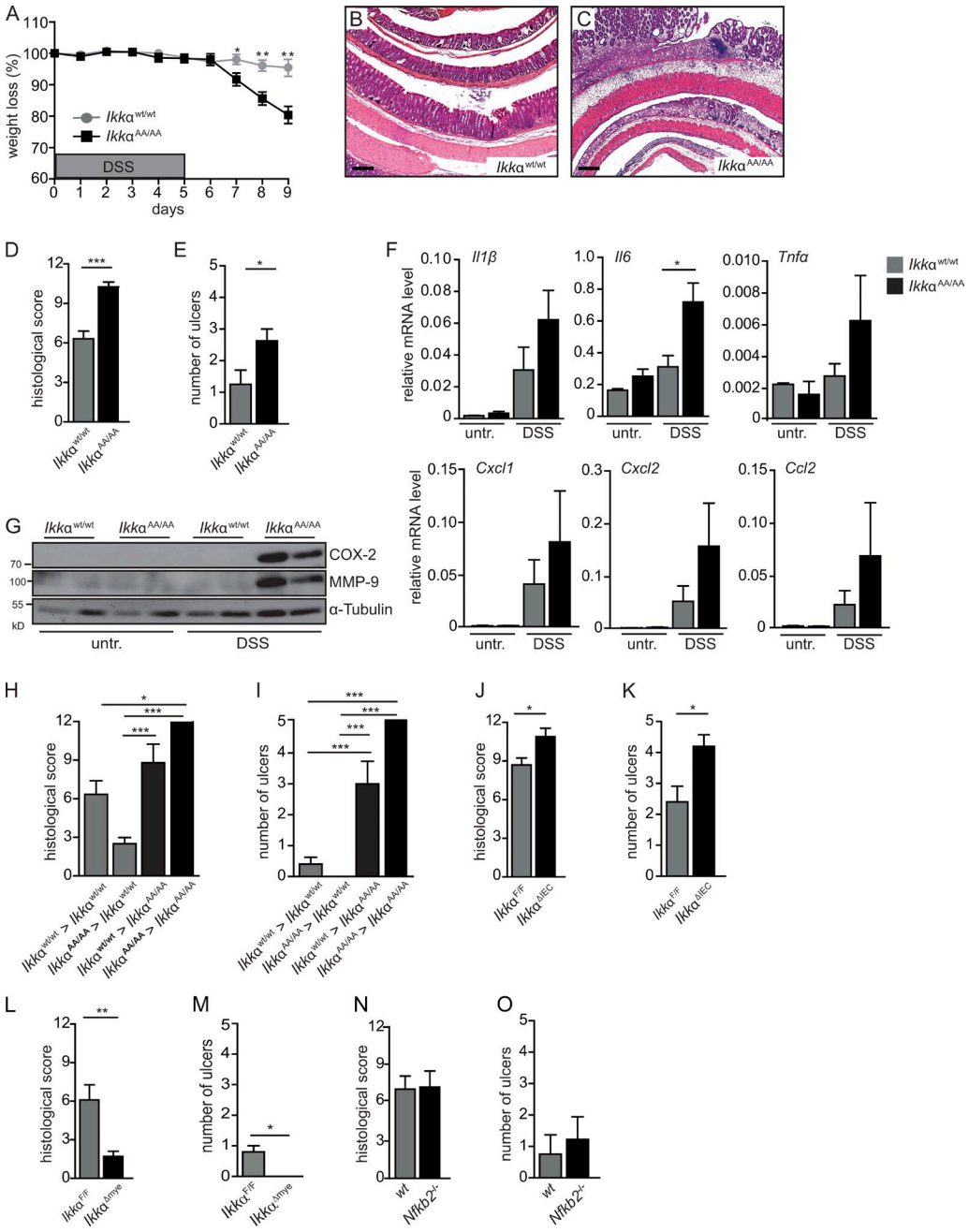

Figure 1. **Epithelial IKKα signaling is essential for tissue repair after DSS-induced injury.** (A) Body weight was determined daily in $Ikk\alpha^{Wt/Wt}$ and $Ikk\alpha^{AA/AA}$ mice treated with 3.5% DSS in drinking water for 5 d, followed by a 4-d recovery phase on normal drinking water. Data are representative of two experiments. $n = 8$. Student's t test was used. (B and C) Representative H&E staining of colon sections from $Ikk\alpha^{Wt/Wt}$ (B) and $Ikk\alpha^{AA/AA}$ (C) mice treated with DSS for 5 d and analyzed on day 9. Bars, 500 µm. (D and E) Quantification of histological damage (D) and number of ulcers (E) on day 9 of the colitis model. $n = 8$. Student's t test was used. (F) Relative mRNA expression levels of inflammatory mediators in the colonic mucosa of untreated (untr.) and DSS-treated mice were determined by quantitative RT-PCR (qRT-PCR). Data are representative of two experiments. $n > 3$. (G) Protein lysates were prepared from whole colonic mucosa from untreated and DSS-treated $Ikk\alpha^{Wt/Wt}$ and $Ikk\alpha^{AA/AA}$ mice on day 9 of the DSS model and were analyzed by immunoblot analysis using the indicated antibodies. (H and I) Histological damage (H) and number of ulcers (I) on day 9 of the colitis model in the indicated bone marrow chimeras (i.e., $Ikk\alpha^{Wt/Wt} > Ikk\alpha^{Wt/Wt}$ indicates $Ikk\alpha^{Wt/Wt}$ bone marrow transplanted into $Ikk\alpha^{Wt/Wt}$ recipients). Data are from two independent experiments. $n \geq 5$. ANOVA followed by Bonferroni posthoc test for multiple datasets was used. (J–O) Histological damage (J, L, and N) and number of ulcers (K, M, and O) in $Ikk\alpha^{F/F}$ and $Ikk\alpha^{\Delta IEC}$ (J and K), in $Ikk\alpha^{F/F}$ and $Ikk\alpha^{\Delta mye}$ (L and M), and $Nf\kappa B2^{+/+}$ and $Nf\kappa B2^{-/-}$ (N and O) mice on day 9 of the DSS regimen. $n > 8$. Student's t test was used. Data are mean ± SEM. *, $P < 0.05$; **, $P < 0.01$; ***, $P < 0.001$.

Ikkα-mutant epithelia was not the consequence of a DSS-dependent general hyperinflammatory reaction in vivo associated with increased proinflammatory cytokine release but, rather, caused by a cell autonomous mechanism, we isolated primary colonic organoids from $Ikk\alpha^{AA/AA}$ and $Ikk\alpha^{Wt/Wt}$ mice. Similarly to the changes observed in vivo, Grp78 and IRE1α expression and *Xbp1* splicing as well as cleaved caspase 12 expression were elevated in ex vivo–cultured organoids (Fig. 2, H and I) confirming an IEC-intrinsic regulation of the ER stress response. Caspase 12 has been suggested to repress the inflammasome thereby blocking processing of IL-1β and IL-18, and accordingly, caspase 12 deficiency improves acute and chronic DSS colitis (Dupaul-Chicoine et al., 2010). IL-18 is mainly secreted by IECs in response to DSS, whereas immune cells are the main IL-1β source (Fig. 3 A). IL-18 as well as IL-18R knockout mice are highly susceptible to DSS-induced colitis (Takagi et al., 2003), and IL-18 supports epithelial cytoprotection during the early phase of wound healing after DSS treatment (Dupaul-Chicoine et al., 2010; Zaki et al., 2010; Elinav et al., 2011). Therefore, we examined serum IL-18 levels in unchallenged or DSS-treated $Ikk\alpha^{AA/AA}$ and $Ikk\alpha^{Wt/Wt}$ mice. In line with enhanced caspase 12 activation in IECs, which should block IL-18 processing, serum IL-18 was significantly lower in $Ikk\alpha^{AA/AA}$ mice during acute colitis (Fig. 3 B). Similar results were obtained in $Ikk\alpha^{\Delta IEC}$ mice (Fig. 3 C), suggesting that impaired IL-18 secretion by *Ikkα*-mutant IECs caused tissue destruction and inflammation during DSS colitis. In line with this notion, administration of recombinant IL-18 prevented weight loss and tissue damage as well as up-regulation of proinflammatory cytokine and chemokine gene expression in whole mucosa of $Ikk\alpha^{AA/AA}$ mice confirming a dampened inflammatory response (Fig. 3, D–I). To further corroborate that impairment of IL-18 secretion causing aggravation of acute colitis was indeed caspase 12 dependent, we generated $Ikk\alpha^{AA/AA}/casp12^{-/-}$ compound mutants. Expectedly, *casp12* deletion improved significantly all parameters of acute colitis in $Ikk\alpha^{AA/AA}$ mice (Fig. 3, J–Q). Collectively, these results suggested that IKKα protects IECs from enhanced ER stress thereby preventing caspase 12 activation and subsequently supports cytoprotective IL-18 production.

IKKα controls stabilization of ATG16L1

A single-nucleotide polymorphism encoding a missense variant in the autophagy gene ATG16L1 (dbSNP accession no. rs2241880; Thr300Ala) is strongly associated with the incidence of CD (Hampe et al., 2007). Moreover, impaired ATG16L1 function has been linked to enhanced IRE1α-dependent splicing of *Xbp1* and Grp78 accumulation in IECs causing increased susceptibility to DSS-induced colitis (Adolph et al., 2013). Considering that ATG16L2, an ATG16L1 isoform, interacts with IKKα in pancreatic epithelial cells (Li et al., 2013) prompted us to investigate a possible connection between IKKα and ATG16L1 in IECs. Hypomorphic expression or loss of ATG16L1 in mice and men is associated with Paneth cell granule abnormalities (Cadwell et al., 2008; Adolph et al., 2013; Lassen et al., 2014) and goblet cell alterations in the colon (Lassen et al., 2014). Comparable abnormalities could be detected in $Ikk\alpha^{AA/AA}$ mice. Immunohistochemical as well as electron microscopical analysis of ileum sections revealed a significant decrease in the number of Paneth cell granules (Fig. 4, A–G), and alcian blue stainings confirmed enlarged goblet cells in $Ikk\alpha^{AA/AA}$ mice (Fig. 4, H and I). The $Atg16l1^{T300A}$ risk variant is highly susceptible to proteolytic degradation by caspase 3 in response to signals from cell-surface death receptors (Lassen et al., 2014; Murthy et al., 2014). Indeed, processing of ATG16L1 was enhanced in $Ikk\alpha^{AA/AA}$-mutant IECs upon DSS challenge accompanied by p62 accumulation (Fig. 4 J). Similarly, TNF stimulation led to enhanced ATG16L1 degradation in the presence of cycloheximide in $Ikk\alpha^{AA/AA}$ colonic organoids compared with $Ikk\alpha^{Wt/Wt}$ colonic organoids, which could be prevented by the pan-caspase inhibitor zVAD (Fig. 4 K). These data strongly suggested that $Ikk\alpha^{AA/AA}$-mutant mice phenocopied *Atg16l1* hypomorphic or $Atg16l1^{T300A}$ knockout animals regarding DSS-induced inflammatory response and Paneth and goblet cell morphology as well as susceptibility to TNF-induced caspase-dependent degradation of ATG16L1. Collectively, these data are raising the possibility that ATG16L1 might be a direct substrate for IKKα phosphorylation. In line with this notion, coimmunoprecipitation confirmed binding of FLAG-tagged IKKα to mCherry-ATG16L1 in HEK293T cells (Fig. 5 A), as well as endogenous IKKα to ATG16L1 in *Wt* colonic organoids upon TNF stimulation (Fig. 5 B). Moreover, glutathione S-transferase (GST) pull-down assays using different GST-ATG16L1 fragments indicated that IKKα interacted with the N-terminal GST-ATG16L1(1–230) and C-terminal GST-ATG16L1(358–607) domains (Fig. 5, C and D). Furthermore, an in vitro kinase assay using lysates from FLAG-$IKK\alpha^{Wt}$ or FLAG-$IKK\alpha^{AA}$ overexpressing HEK293T cells confirmed an IKKα-dependent phosphorylation of the GST-ATG16L1(231–352) substrate that contains the consensus caspase cleavage sites flanking T300 (Murthy et al., 2014) as well as several additional putative phosphorylation sites (Fig. 5 E). Subsequent mass-spectrometric analysis revealed three phosphorylated serines (S278, S287, and S289; Fig. 5 F). Site-directed mutagenesis confirmed lack of phosphorylation in the GST-ATG16L1(231–352)^{S278A} mutant but not when the other two serine residues were mutated to alanine (Fig. 5 G). Moreover, TNF stimulation of endogenous $Ikk\alpha^{Wt/Wt}$ or $Ikk\alpha^{AA/AA}$ in colonic organoids revealed marked IKKα-dependent phosphorylation of GST-ATG16L1(231–352) (Fig. 5 H). Importantly, overexpression of mCherry-tagged ATG16L1^{S278A} in HeLa cells led to enhanced caspase-dependent degradation in response to TNF stimulation, which was comparable with the extent of degradation observed in ATG16L1^{T300A}-mutant cells (Fig. 5 I). This was further confirmed when both ATG16L1 mutants and *Wt* ATG16L1 were cleaved directly by caspase 3 (Fig. 5 J). Collectively, these data confirmed the direct regulatory function of IKKα

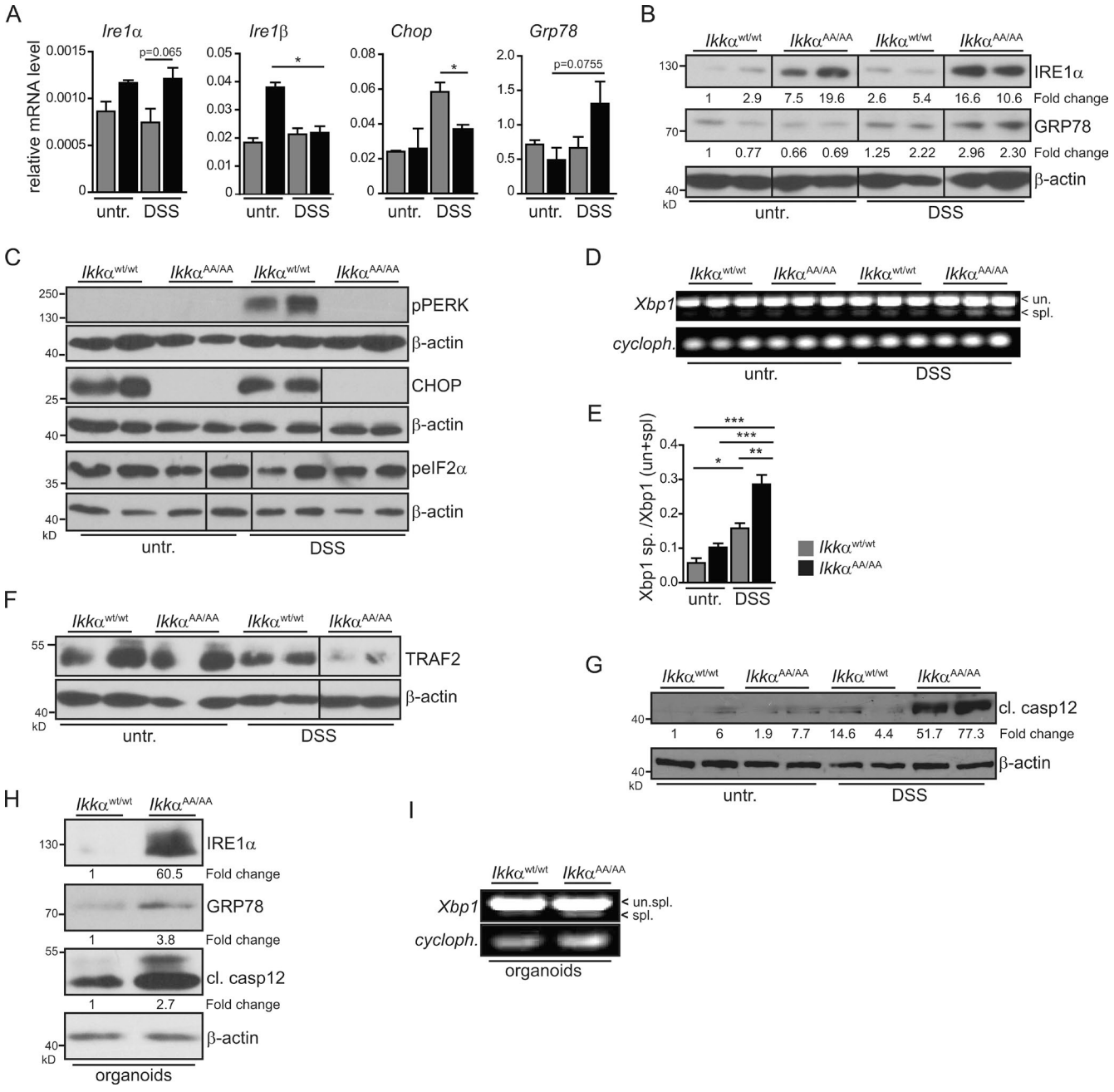

Figure 2. **Induction of the IRE1α/*Xbp1* branch of the UPR in *Ikkα*$^{AA/AA}$ enterocytes.** (A) Relative expression levels of genes involved in control of the UPR in isolated colonic epithelia from *Ikkα*$^{Wt/Wt}$ and *Ikkα*$^{AA/AA}$ mice that were either left untreated (untr.) or fed with 3.5% DSS for 3 d determined by qRT-PCR. Data are presented as mean ± SEM from one of two experiments performed. $n = 3$. *, $P < 0.05$. (B) Colonic epithelia were obtained from *Ikkα*$^{Wt/Wt}$ and *Ikkα*$^{AA/AA}$ mice that were either left untreated or fed with 3.5% DSS for 3 d, and protein lysates were prepared. Samples were analyzed by immunoblot analysis using the indicated antibodies. Data are representative of greater than two experiments. (C) IECs were obtained from *Ikkα*$^{Wt/Wt}$ and *Ikkα*$^{AA/AA}$ mice left untreated or treated with DSS for 3 d, and protein lysates were prepared. Protein expression was analyzed by immunoblot analysis using the indicated antibodies. (D) *Xbp1* mRNA splicing in colonic epithelial cells at day 0 and day 3 of DSS treatment determined by PCR. (E) Densitometric quantification of the ratio of spliced versus unspliced *Xbp1* in colonic epithelial cells. Data are presented as mean ± SEM from one of two experiments performed. $n = 3$. *, $P < 0.05$; **, $P < 0.01$; ***, $P < 0.001$ by ANOVA followed by Bonferroni posthoc test for multiple datasets. (F and G) Immunoblot analysis of the indicated proteins in lysates prepared from colonic epithelial cells obtained from *Ikkα*$^{Wt/Wt}$ and *Ikkα*$^{AA/AA}$ mice left untreated of treated with DSS for 3 d. (H) Protein expression levels in lysates from unstimulated colonic organoids from *Ikkα*$^{Wt/Wt}$ and *Ikkα*$^{AA/AA}$ mice. Data are representative of two experiments. (I) *Xbp1* mRNA splicing in unchallenged colon organoids from *Ikkα*$^{Wt/Wt}$ and *Ikkα*$^{AA/AA}$ mice determined by PCR. Data are representative of two experiments. cl., cleaved; cycloph., cyclophilin; spl., spliced; un., unspliced.

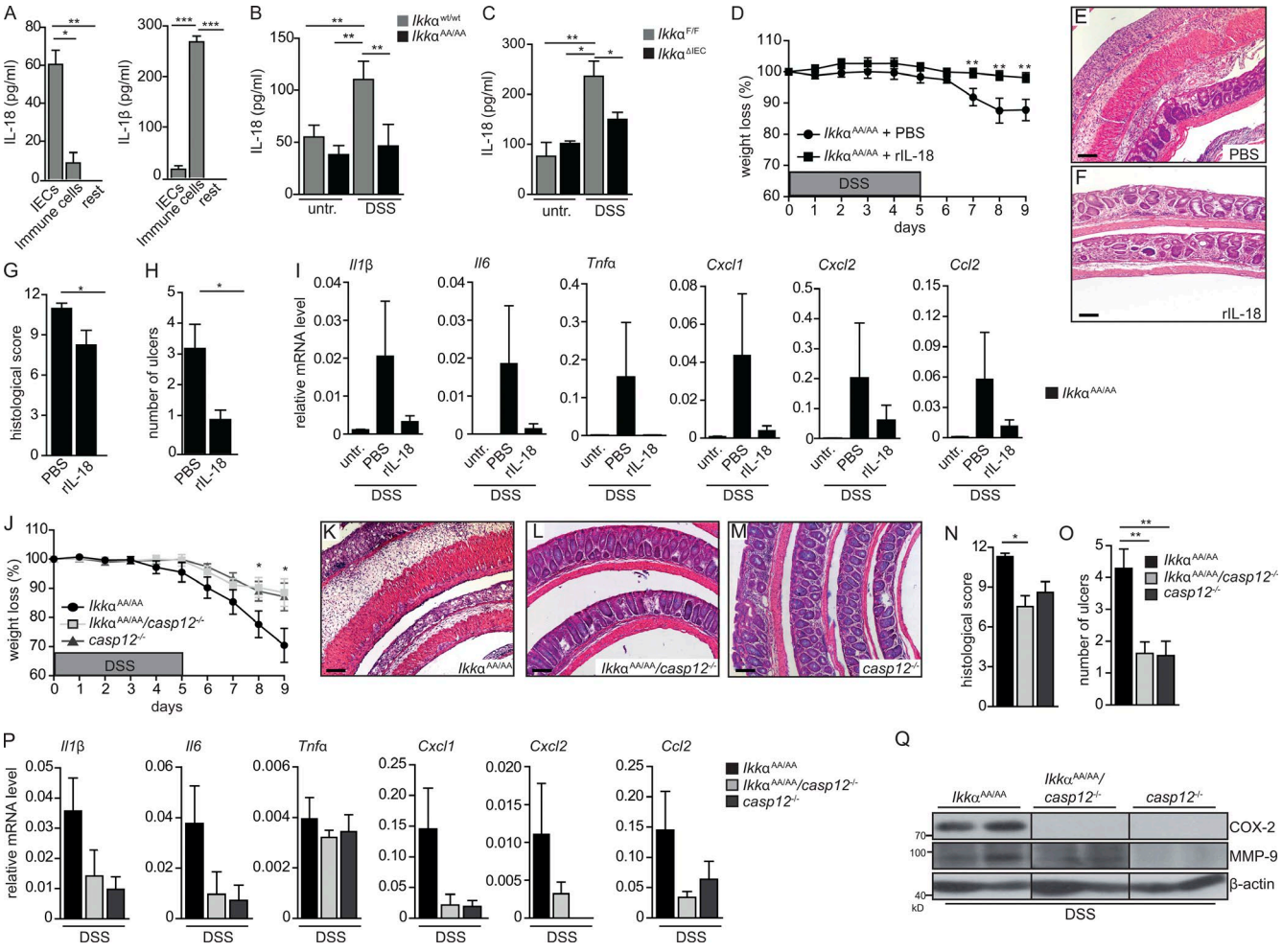

Figure 3. **Enhanced caspase 12 activation and decreased cytoprotective IL-18 serum levels in *Ikkα*$^{AA/AA}$ mice.** (A) Quantification of ex vivo production of IL-18 and IL-1β by flow cytometry–sorted IECs and immune cells from the colon of WT mice on day 5 of 3.5% DSS treatment. IECs were defined as CD45$^-$, CD11b$^-$, Gr1$^-$, and EpCAM$^+$; immune cells as CD45$^+$, CD11b$^+$, Gr1$^+$, and EpCAM$^-$; and rest as CD45$^-$, CD11b$^-$, Gr1$^-$, and EpCAM$^-$. $n = 5$. ANOVA followed by Bonferroni posthoc test for multiple datasets was used. (B) Serum IL-18 levels in *Ikkα*$^{Wt/Wt}$ and *Ikkα*$^{AA/AA}$ mice on days 0 and 9 of DSS (3.5%) regimen. Data are from two independent experiments. $n > 6$. ANOVA followed by Bonferroni posthoc test for multiple datasets was used. (C) Serum IL-18 levels were determined by ELISA from *Ikkα*$^{F/F}$ and *Ikkα*$^{\Delta IEC}$ mice at days 0 and 9 of DSS (3.5%) regimen. $n = 5$. ANOVA followed by Bonferroni posthoc test for multiple datasets was used. (D) Body weight was determined in *Ikkα*$^{AA/AA}$ mice during DSS (3.5%)-induced acute colitis. Mice were daily i.p. injected either with PBS or recombinant IL-18 (rIL-18; 0.5 µg/d). Data are from two independent experiments. $n > 8$. Student's *t* test was used. (E and F) Representative H&E-stained colon sections from *Ikkα*$^{AA/AA}$ mice treated with PBS (E) or rIL-18 (F) throughout the 3.5% DSS regimen. Bars, 500 µm. (G and H) Histological damage (G) and number of ulcers (H) on day 9 of DSS regimen in *Ikkα*$^{AA/AA}$ mice that had been injected daily either with PBS or rIL-18. Data are from two independent experiments. $n > 7$. Student's *t* test was used. (I) Relative mRNA expression levels of inflammatory mediators in the colon of *Ikkα*$^{AA/AA}$ mice that were left untreated or received either PBS or rIL-18 for nine consecutive days and analyzed on day 9 of the 3.5% DSS regimen. Data are from two independent experiments. $n > 3$. (J) Body weight was determined in *Ikkα*$^{AA/AA}$, *Ikkα*$^{AA/AA}$*casp12*$^{-/-}$, and *casp12*$^{-/-}$ mice during DSS (2.5%)-induced colitis. Data are from one of two experiments performed. $n > 5$. Student's *t* test was used. (K–M) Representative H&E staining of colon sections from *Ikkα*$^{AA/AA}$ (K), *Ikkα*$^{AA/AA}$*casp12*$^{-/-}$ (L), and *casp12*$^{-/-}$ (M) mice treated with 2.5% DSS for 5 d and analyzed on day 9. Bars, 500 µm. (N and O) Histological damage (N) and number of ulcers (O) in *Ikkα*$^{AA/AA}$, *Ikkα*$^{AA/AA}$*casp12*$^{-/-}$, and *casp12*$^{-/-}$ mice on day 9 of the DSS regimen. Data are from one of two experiments performed. $n > 5$. Student's *t* test was used. (P) Relative mRNA expression levels of inflammatory mediators in the colon of *Ikkα*$^{AA/AA}$, *Ikkα*$^{AA/AA}$*casp12*$^{-/-}$, and *casp12*$^{-/-}$ mice on day 9 of DSS (2.5%) regimen were determined by qRT-PCR. $n > 3$. (Q) Whole colonic lysates were prepared from *Ikkα*$^{AA/AA}$, *Ikkα*$^{AA/AA}$*casp12*$^{-/-}$, and *casp12*$^{-/-}$ mice on day 9 of the 2.5% DSS treatment, and protein expression was analyzed by immunoblot analysis using the indicated antibodies. Data are mean ± SEM. *, $P < 0.05$; **, $P < 0.01$; ***, $P < 0.001$. untr., untreated.

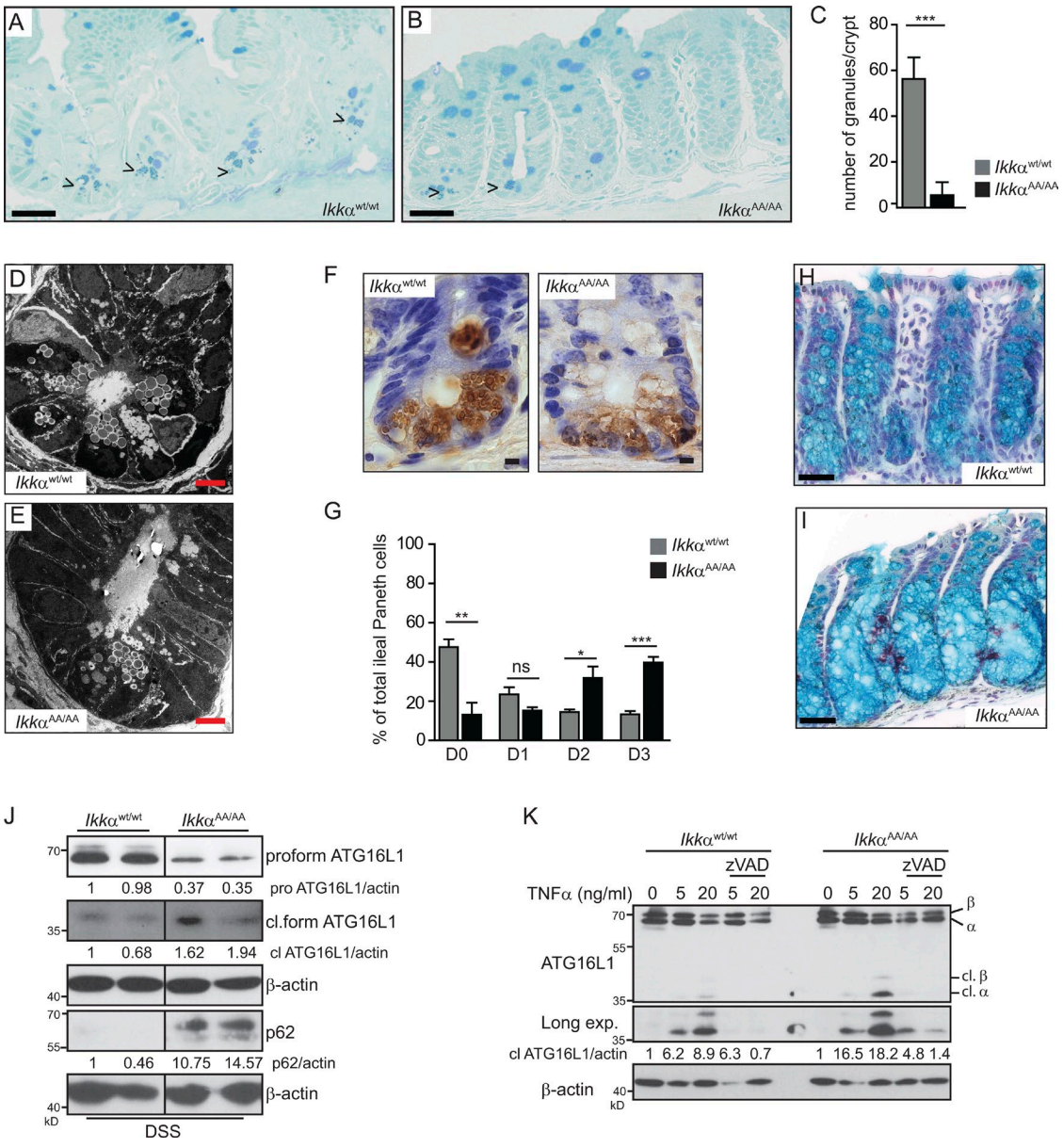

Figure 4. ***Ikkα*$^{AA/AA}$ mice phenocopy ATG16l1-mutant mice.** (A and B) Representative methylene blue staining of ileum sections from *Ikkα*$^{Wt/Wt}$ (A) and *Ikkα*$^{AA/AA}$ (B) mice. Arrowheads indicate secretory granules in Paneth cells. Bars, 50 µm. (C) Quantification of Paneth cells in the ileal crypts from *Ikkα*$^{Wt/Wt}$ and *Ikkα*$^{AA/AA}$ mice according to the number of methylene blue–positive granular vesicles. Data are mean ± SEM. n = 10 crypts counted. ***, P < 0.001. (D and E) Representative transmission electron microscopic images showing Paneth cells from *Ikkα*$^{Wt/Wt}$ (D) and *Ikkα*$^{AA/AA}$ (E) mice indicating decreased number of secretory granules in *Ikkα*$^{AA/AA}$ Paneth cells. Bars, 5 µm. (F) Immunohistochemical staining for lysozyme in paraffin-embedded ileal crypt sections from unchallenged *Ikkα*$^{Wt/Wt}$ and *Ikkα*$^{AA/AA}$ mice reveals defective secretory granule formation in *Ikkα*$^{AA/AA}$ Paneth cells. Bars, 10 µm. (G) Lysozyme expression was quantified according to Cadwell et al. (2008): normal (D0), disordered (D1), depleted (D2), and diffuse (D3). n = 411 cells from four *Ikkα*$^{Wt/Wt}$ and n = 370 cells from four *Ikkα*$^{AA/AA}$ mice. Data are mean ± SEM from two independent experiments. *, P < 0.05; **, P < 0.01; ***, P < 0.001 by Student's t test. (H and I) Representative images of colon sections of *Ikkα*$^{Wt/Wt}$ (H) and *Ikkα*$^{AA/AA}$ (I) mice stained with alcian blue to visualize goblet cells. Bars, 50 µm. (J) Lysates of isolated IECs, from 3.5% DSS–treated *Ikkα*$^{Wt/Wt}$ and *Ikkα*$^{AA/AA}$ mice for 3 d, were prepared, and samples were analyzed by Western blotting with the indicated antibodies. Data are representative of two experiments. (K) ATG16L1 proteolytic cleavage was assessed by immunoblot analysis in colonic organoids. Organoids were pretreated with DMSO or pan-caspase inhibitor (zVADfmk), followed by TNF stimulation in the presence of 10 µg/ml cycloheximide for 3 h. Data are representative of two experiments. cl., cleaved; exp., exposure.

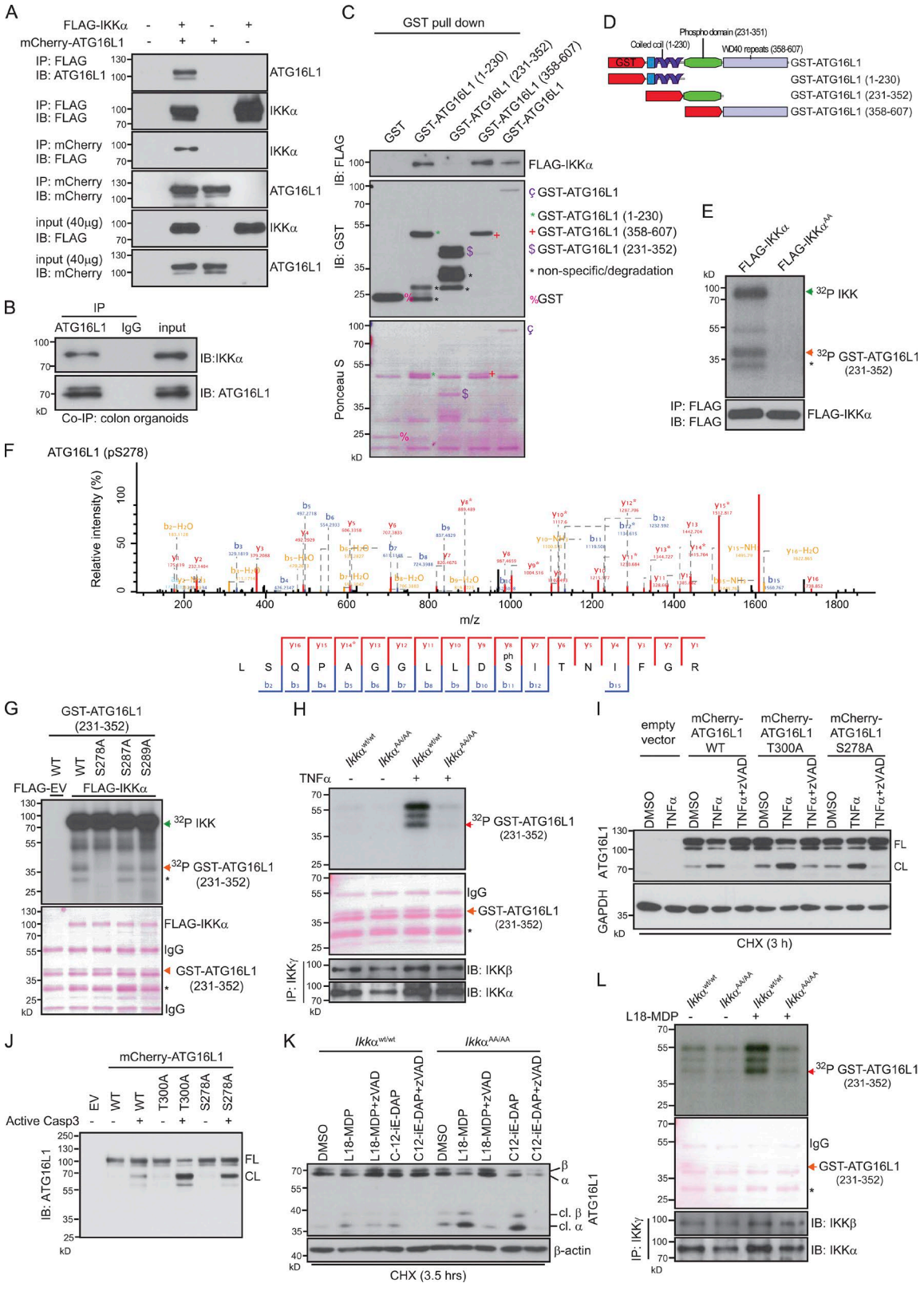

Figure 5. **IKKα phosphorylates ATG16L1.** (A) Coimmunoprecipitation (Co-IP) and immunoblot (IB) analysis showing interaction of FLAG-IKKα and mCherry-ATG16L1. HEK293T cells were transfected as indicated, and lysates were subjected to coimmunoprecipitation assays. Immunoblots from 40-μg input were used to examine protein expression levels. (B) Coimmunoprecipitation of endogenous IKKα and ATG16L1 in WT colonic organoids. 600 μg of

in phosphorylating ATG16L1 resulting in its stabilization and decreased susceptibility to caspase-dependent degradation.

Recently, activation of NOD2, an intracellular pattern-recognition receptor that recognizes muramyldipeptide (MDP), an integral component of bacterial cell walls, has been implicated in autophagosome formation depending in part on ATG16L1 (Homer et al., 2010; Travassos et al., 2010). Moreover, *NOD2* gene polymorphisms markedly increase susceptibility to CD (Hugot et al., 2001; Wehkamp et al., 2004), and NOD2 can activate the IKK complex (Abbott et al., 2004; Schroder and Tschopp, 2010). Therefore, we tested whether activation of NOD2 may affect ATG16L1 stability in an IKKα-dependent manner and stimulated colonic organoids with either NOD2 agonist L18-MDP or NOD1 activating C12-iE-DAP. Both treatments led to markedly enhanced ATG16L1 degradation in IKKα-mutant colonic organoids (Fig. 5 K). Furthermore, activation of NOD2 led to an IKKα-dependent phosphorylation of GST-ATG16L1(231–352) (Fig. 5 L).

DISCUSSION

Recent genome-wide association studies identified a single-nucleotide polymorphism in the autophagy gene *ATG16L1* that is strongly associated with the incidence of CD (Hampe et al., 2007; Rioux et al., 2007). ATG16L1^{T300A} is more sensitive to caspase 3–mediated cleavage and degradation and, consequently, results in impaired autophagy in response to cellular stress (Lassen et al., 2014; Murthy et al., 2014). The Thr300 is located in a region with several additional putative phosphorylation sites. However, upstream kinases have not been identified so far. Here, we show that IKKα phosphorylates ATG16L1 at the Ser278 residue but not at Thr300, suggesting that several phosphorylation sites in this region are involved in the stabilization of ATG16L1.

Similar to the ATG16L1^{T300A} polymorphism, *NOD-2* gene polymorphisms, which result in loss of protein function, are associated with increased risk of developing CD (Hugot et al., 2001; Wehkamp et al., 2004). NOD1 and NOD2 recruit ATG16L1 to the plasma membrane at the site of bacterial entry independently of IKK activation (Travassos et al., 2010), but it is not clear whether this function is directly regulated through the interaction of both proteins at the endogenous level, as overexpressed NOD1 and NOD2 were shown to interact with ATG16L1. Furthermore, ATG16L1 negatively regulates NOD1- and NOD2-driven cytokine responses in an autophagy-independent manner (Sorbara et al., 2013). Interestingly, NOD stimulation can also activate the IKK complex (Abbott et al., 2004; Schroder and Tschopp, 2010). Our data now show that NOD signaling is involved in ATG16L1 phosphorylation and stabilization through IKKα, thus challenging the concept that interaction of NOD2 and ATG16L1 occurs in an IKK-independent manner (Travassos et al., 2010). Thus, IKKα appears to comprise a central regulatory kinase that mediates the stabilization of ATG16L1 in response to various extracellular stimuli, indicating that IKKα is a critical link between NOD signaling and ATG16L1 during acute inflammation.

The IKKα-dependent ATG16L1 stabilization confers an important regulatory mechanism in the control of autophagic protein degradation. In fact, various studies have highlighted the regulation of autophagy by IKKβ/NF-κB or vice versa. TNF-dependent activation of NF-κB suppresses

protein lysates from colon organoids were immunoprecipitated with ATG16L1 or control IgG. The immunoprecipitates and 40 µg of input lysates were analyzed by immunoblot analysis using the indicated antibodies. Data are representative of two experiments. (C) HEK293T cells were transfected with FLAG-IKKα, and whole-cell extracts were subjected to a pull down assay using various forms of GST-ATG16L1 and GST-Sepharose beads. The bead-bound proteins were analyzed by immunoblot analysis using anti-FLAG antibody. Data are representative of two experiments. (D) Schematic representation of the full-length ATG16L1 and different construct domains used for the expression of GST-fusion proteins. (E) HEK293T cells were transfected with FLAG-IKKα^{Wt} or FLAG-IKKα^{AA}. After 48 h, the cells were collected and lysed, and whole-cell extracts were subjected to immunoprecipitation using protein A/G plus agarose beads and anti-FLAG antibody. Then, immunoprecipitates were subjected to in vitro kinase assay with GST-ATG16L1(231–352). The FLAG immunoblot shows equal amounts of immunopurified FLAG-IKKα^{Wt} or FLAG-IKKα^{AA}. Phosphorylation of GST-ATG16L1(231–352) was confirmed by mass spectrometry. Data are representative of three experiments. (F) Mass spectrometric fragment ion scan of the peptide corresponding to phosphorylated serine 278 in ATG16L1. Data are representative of two experiments. (G) In vitro kinase assay of FLAG-IKKα^{Wt} overexpressing HEK293T cells and different point-mutated GST-ATG16L1(231–352) substrates. Phosphorylated GST-ATG16L1(231–352) was visualized by autoradiography. Ponceau S staining shows the equal amounts of GST-ATG16L1 substrates. Data are representative of two experiments. EV, empty vector. (H) Endogenous IKK complex was immunoprecipitated using anti-IKKγ from untreated or 20 ng/ml TNF–treated (15 min) colonic organoids isolated from *Ikkα$^{Wt/Wt}$* and *Ikkα$^{AA/AA}$* mice and then subjected to in vitro kinase assay using GST-ATG16L1(231–352) as a substrate. Phosphorylated GST-ATG16L1(231–352) was visualized by autoradiography. Ponceau S staining and immunoblotting against IKKα and IKKβ show the equal amount of GST-ATG16L1 and immunoprecipitation efficiency, respectively. Data are representative of two experiments. (I) ATG16L1 proteolytic cleavage was assessed by immunoblot analysis in HeLa cells expressing mCherry-ATG16L1 Wt and mutants. HeLa cells were pretreated for 1 h with DMSO or 10 µM pan-caspase inhibitor (zVADfmk), followed by TNF stimulation (20 ng/ml) in the presence of 10 µg/ml cycloheximide (CHX) for 3 h. (J) Caspase 3–mediated in vitro ATG16L1 cleavage was assessed by immunoblot analysis. mCherry-ATG16L1 *Wt* and mutants were immunoprecipitated from HEK293T cells. Then, immunoprecipitates were subjected to in vitro cleavage assay using recombinant active caspase 3. Data are representative of two experiments. (I and J) CL, cleaved; FL, full length. (K) ATG16L1 proteolytic cleavage was assessed by immunoblot analysis in colonic organoids. Organoids were pretreated with DMSO or pan-caspase inhibitor (zVADfmk), followed by stimulation with NOD ligands, 20 µg/ml L-18MDP, and 20 µg/ml C12-iE-DAP, in the presence of 10 µg/ml cycloheximide for 3.5 h. Data are representative of two experiments. cl., cleaved. (L) Endogenous IKK complex was immunoprecipitated from untreated or L18-MDP–treated (20 µg/ml for 15 min) colonic organoids and then subjected to in vitro kinase assay as described in H. Data are representative of two experiments. (G, H, and L) Single asterisks indicate nonspecific signal determined by mass spectrometry.

autophagy in several cancer cells (Djavaheri-Mergny et al., 2006). Similarly, IKKβ/NF-κB signaling negatively regulates starvation-induced autophagy in cells from acute myeloid leukemia and myelodysplastic syndrome patients (Fabre et al., 2007). Moreover, autophagy can also negatively regulate the NF-κB pathway by mediating the degradation of α, β, and γ subunits of the IKK complex and of its upstream activator of NF-κB–inducing kinase (Qing et al., 2007). Interestingly, activation of NF-κB can enhance autophagy during heat shock recovery to increase cell survival (Nivon et al., 2009). In addition, IKK activation is sufficient to promote autophagy independently of NF-κB signaling (Criollo et al., 2010; Comb et al., 2011). Thus, regulation of autophagy by IKK/NF-κB signaling is regulated in a strict context-dependent manner. Recently, it was shown that loss of IKKα function but not IKKβ in pancreatic acinar cells results in impaired autophagy because of substantial increase of p62 and subsequent accumulation of ER stress, which finally leads to spontaneous pancreatitis (Li et al., 2013). Deletion of p62 rescued the IKKα-dependent phenotypes, indicating the crucial link between IKKα and p62 during autophagic induction and ER stress in the pancreas (Li et al., 2013). Similarly, during DSS-induced acute colitis, mutant IKKα IECs express markedly elevated levels of p62. However, in stark contrast to the phenotype observed during pancreatitis, loss of p62 is dispensable for induction of ER stress in IKKα mutants during colitis (unpublished data) suggesting that other selective autophagy receptors such as optineurin or NDP52 may be involved in this link.

We show that IKKα protects mice from enhanced UPR during DSS-induced colitis by specifically controlling the IRE1α-dependent UPR signaling cascade. The expression of Grp78, IRE1α, and Xbp1 splicing was elevated in the colonic organoids from IKKα mutants, suggesting IEC-intrinsic regulation of the ER stress response by IKKα. Recently, a link between ER stress and the IKK complex has been suggested. However, it was demonstrated that enhanced ER stress impairs classical NF-κB activation, which is the diametric opposite phenotype of what we describe here, namely an enhanced UPR in the absence of IKKα kinase function. Elevated ER stress, IRE1 up-regulation, and TRAF2 degradation are involved in IRE1α-dependent caspase 12 activation (Yoneda et al., 2001; Hu et al., 2006). Caspase 12 is a negative regulator of caspase 1 activation and thereby blocks the processing of IL-1β and IL-18 (Dupaul-Chicoine et al., 2010) and enhances vulnerability to bacterial infection and septic shock (Saleh et al., 2006). Several studies have confirmed a cytoprotective role of IL-18 during epithelial regeneration after DSS-induced injury (Dupaul-Chicoine et al., 2010; Zaki et al., 2010; Elinav et al., 2011), and indeed, recombinant IL-18 administration or deletion of caspase 12 in IKKα mutants significantly improved all the parameters observed upon DSS-induced colitis. Recently, it was suggested that IKKα signaling in IECs is required for innate lymphoid 3 cell (ILC3) recruitment

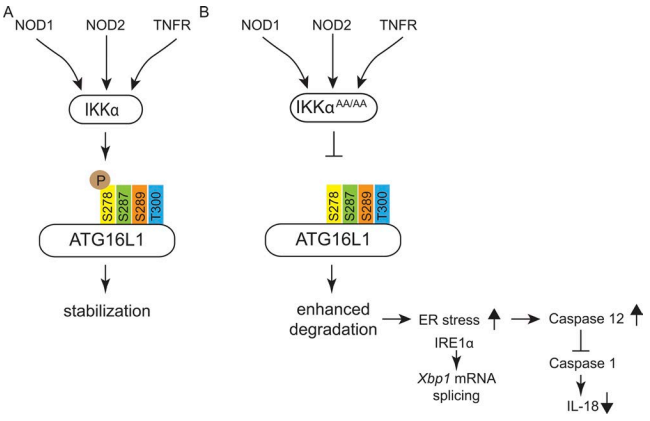

Figure 6. **Model summarizing the proposed signaling events in IKKα–mutant mice.** (A) Both NOD and TNF-R engagements activate IKKα. Activated IKKα phosphorylates ATG16L1 specifically at Ser278 and protects it from caspase 3–dependent cleavage leading to its stabilization. (B) In the absence of IKKα activity (*Ikkα*$^{AA/AA}$), caspase-dependent cleavage of ATG16L1 is enhanced because of lack of phosphorylation of ATG16L1 at Ser278 by IKKα impairing autophagic protein degradation. As a consequence, ER stress–induced IRE1α overexpression is associated with elevated levels of active caspase 12, which results in the inhibition of caspase 1 activity and lower levels of IL-18. Decreased levels of IL-18 cause retarded epithelial regeneration and enhanced inflammation.

and up-regulation of IL-22 in the intestinal mucosa during *C. rodentium* infection. This was suggested to be dependent on elevated *Tslp* expression in IKKα-deficient IECs. Considering that IEC-derived IL-18 is also required for IL-22 expression in ILCs upon *Toxoplasmosis gondii* infection (Muñoz et al., 2015), our data suggest that the decreased IL-18 secretion in IKKα-deficient IECs we observe here may contribute to lower IL-22 expression in the mucosa of IKKα-mutant mice as well.

In summary, we propose IKKα to be the central kinase controlling ATG16L1 function by mediating the response to a whole range of various extracellular stimuli during inflammation (Fig. 6). Activation of this signaling axis stabilizes ATG16L1 and prevents ER stress, culminating in a novel antiinflammatory cytoprotective mechanism that may be engaged to counteract the proinflammatory actions triggered by canonical IKK/NF-κB activation. Our data suggest that various phosphorylation sites in ATG16L1 are involved in this process considering that both the T300 and the S278 residues control sensitivity of ATG16L1 to caspase 3–mediated cleavage. NOD1 and NOD2 have been shown to directly interact with ATG16L1 by recruiting it to the site of bacterial entry (Travassos et al., 2010). We now provide evidence that, additionally, NOD proteins are involved in ATG16L1 stabilization via IKKα, thus challenging the concept that interaction of NOD2 and ATG16L1 occurs in an IKK-independent manner (Travassos et al., 2010) and possibly placing IKKα as the missing link between NOD and ATG16L1 in IBD pathogenesis.

MATERIALS AND METHODS

Mice

Ikkα$^{AA/AA}$ knock-in has been previously described (Cao et al., 2001). To delete exons 6–9 of *Ikkα* in IECs and myeloid cells, we crossed floxed *Ikkα* mice (Takeda et al., 1999) to *villin*-Cre (Madison et al., 2002) and *LysM-Cre* (Clausen et al., 1999) transgenic mice, respectively. All mice, including littermate controls, were crossed on FvB background for at least four generations. *Nfkb2*$^{-/-}$ (provided by R.M. Schmid, Technical University Munich, Munich, Germany; Paxian et al., 2002) and *caspase-12*$^{-/-}$ (Saleh et al., 2006) mice have been previously described. *Ikkα*$^{AA/AA}$*caspase-12*$^{-/-}$ double mutants were kept on a mixed background and were generated by crossing mice heterozygous for the corresponding genes. All mice experiments and procedures were reviewed and approved by the Regierung von Oberbayern.

Colitis induction and histological scoring

Experimental acute colitis was induced by administrating 3.5% DSS (55 kD; MP Biomedicals) in the drinking water for five consecutive days, followed by four additional days of regular drinking water. Mice were euthanized on day 9, and colons were excised, open longitudinally, fixed as Swiss-rolls in 4% paraformaldehyde overnight at 4°C, and embedded in paraffin. Sections were stained with hematoxylin and eosin (H&E) according to standard protocols, and severity of colitis was assessed in a blinded way. The colonic epithelial damage score was assigned as follows: 0, normal; 1, hyperproliferation; 2, mild to moderate loss of crypts, 10–50%; 3, severe loss of crypts, 50–90%; 4, complete loss of crypts, intact epithelium; 5, ulcerated epithelium. The infiltration with inflammatory cells score was assigned separately for: mucosa (0 = normal, 1 = mild, 2 = modest, and 3 = severe), submucosa, and muscle/serosa (0 = normal, 1 = mild to modest, and 2 = severe). The scores for epithelial damage and inflammatory cell infiltration were added, resulting in a total score ranging from 0–12.

Cells and reagents

HEK239T and HeLa cells were transfected with either Viromer red (Lipocalyx) or Lipofectamine 2000 (Thermo Fisher Scientific) for plasmid overexpression. The following reagents were used at final concentrations of: 20 μg/ml L18-MDP (InvivoGen), 20 μg/ml C12-iE-DAP (InvivoGen), 10 μg/ml cycloheximide (Sigma-Aldrich), 10 mM 3-methyladenine (Sigma-Aldrich), 10 μM MG132 (Merck), 20 μM Z-VAD-FMK (EMD Millipore), and 30 μM ML120B (Millennium Pharmaceuticals).

Cloning and site-directed mutagenesis

Generation of Flag-tagged wild-type *Ikkα* and Flag-tagged *Ikkα*^{AA} plasmids has been previously described (Kwak et al., 2000). mCherry-fused human ATG16L1 cDNA was cloned into the pcDNA3.1/hygro(−) vector (Thermo Fisher Scientific) at Xho1 and EcoRV sites. Truncated human ATG16L1 cDNA fragments (amino acids 1–230, 231–352, and 358–607) were cloned into the GST vector pGEX4T1 (GE Healthcare) at EcoR1 and Xho1 sites. Recombinant GST-tagged ATG16L1 fragments were purified from BL21 *Escherichia coli* competent cells using Glutathione Sepharose 4B (GE Healthcare). Full-length GST-tagged human ATG16L1 was purchased from Abnova. Plasmid containing GST-ATG16L1(231–352) and mCherry-ATG16L1 was used for site-directed mutagenesis using a QuikChange Lightning Site-Directed Mutagenesis kit (Agilent Technologies) following the manufacturer's instruction. All mutations were confirmed by direct sequencing and observing individual sequence electropherograms. The primers used for the mutagenesis are as follows: ATG16L1 sense primer (S278A), 5′-GCTGGAGGCCTTCTGGAT**G**CTATCACTAATA TCTTTGGG-3′; ATG16L1 antisense primer (S278A), 5′-CCAAAGATATTAGTGATAG**C**ATCCAGAAGGCC TCCAGC-3′; ATG16L1 sense primer (S287A), 5′-AAT ATCTTTGGGAGACGC**G**CTGTCTCTTCCTTCCCAG TC-3′; ATG16L1 antisense primer (S287A), 5′-GACTGG GAAGGAAGAGACAG**C**GCGTCTCCCAAAGATATT-3′; ATG16L1 sense primer (S289A), 5′-GACTGGGAAGGA AG**C**GACAGAGCGTCTCC-3′; ATG16L1 antisense primer (S289A), 5′-GGAGACGCTCTGTC**G**CTTCCTTCCCAG TC-3′; ATG16L1 sense primer (S278E), 5′-CCTGCTGGA GGCCTTCTGGAT**GAA**ATCACTAATATCTTTGGG AGA-3′; ATG16L1 antisense primer (S287E), 5′-TCT CCCAAAGATATTAGTGAT**TTC**ATCCAGAAGGCC TCCAGCAGG-3′; ATG16L1 sense primer (T300A), 5′-CAGGACAATGTGGAT**G**CTCATCCTGGTTCTGGTA AAGAAGTG-3′; and ATG16L1 antisense primer (T300A), 5′-CACTTCTTTACCAGAACCAGGATGAG**C**ATCCAC ATTGTCCTG-3′. Bold letters indicate the mutated bases.

Protein analysis, antibodies, and immunohistochemistry

IEC isolation and immunoblot and immunoprecipitation analysis were performed as previously described (Cao et al., 2001; Greten et al., 2004). The following antibodies were used for immunoblotting: anti–caspase 12 (2202), anti-CHOP (2895), anti-GRP78 (3177), anti-IRE1α (3294), anti-LC3 (2775), anti-peIF2α (3398), anti-pIκBα (2859), anti-TRAF2 (4724), and anti–pNF-κB p65 (3033) from Cell Signaling Technology; anti–MMP-9 (sc-6840), anti–NF-κB p65 (sc-372), anti-GADPH (sc-32233), and anti–α-tubulin (sc-32293; DM1A) from Santa Cruz Biotechnology, Inc.; anti-COX2 (160106) from Cayman; anti–β-actin (A4700) and anti-FLAG (F1804) from Sigma-Aldrich; anti-IKKα (IMG136A) from Imgenex; anti-p62 (GP62-C) from Progene; anti-p62 (H00008878-MO3) from Abnova; anti-ATG16L1 (M150-3; for immunoblotting) from MBL international; anti-ATG16L1 (ab47946; for immunoprecipitation) from Abcam; anti-pPERK (P3346-01) from US Biologicals; and anti-lysozyme for immunohistological staining from Dako. 3.5-μm paraffin sections were stained using standard immunohistochemical procedures.

In vitro kinase assay

Flag-tagged wild-type *Ikkα* and Flag-tagged $Ikk\alpha^{AA}$ plasmids were overexpressed in HEK293T cells, and IKKα was immunoprecipitated from cells lysates using an anti-Flag antibody. Immunoprecipitated IKKα and 1 μg of recombinant ATG16L1(231–352) Wt, S278A, S287A, and S289A fused to GST were used for in vitro kinase assays in a mixture containing ATP mix solution (10 mM ATP, 100 mM Tris, pH 7.5, 50 mM $MgCl_2$, and 10 mM dithiothreitol [DTT]) and kinase assay buffer (0.25 M Hepes, pH 7.5, 0.1 M $MgCl_2$, 0.25 M β-glycerophosphate, and 1.5 M NaCl). A total of 5 μCi (32P γ-ATP; Hartmann analytic) was used for 30 μl kinase reaction. Kinase reactions were incubated for 30 min at 30°C. The reaction was stopped by adding sample loading buffer, and samples were then boiled, separated by SDS-PAGE, transferred to polyvinylidene fluoride membranes, and visualized by autoradiography.

In vitro cleavage assay

pcDNA3.1 construct of wild-type, T300A, and S278A variants of human ATG16L1 with N-terminal mCherry tag were transfected in HeLa cells using Lipofectamine 2000 following the manufacturer's instruction. 600 μg of total cell lysate and 15 μl of RFP-Trap beads (ChromoTek) were used to immunoprecipitate mCherry-tagged ATG16L1. Then, immunoprecipitates were divided into two equal parts; one part was used to monitor immunoprecipitation efficiency, and the other part was washed twice with 1× caspase activity buffer (MBL international). Finally, immunoprecipitated mCherry-ATG16L1 was subjected to in vitro cleavage assay using 2 U of recombinant active caspase 3 (MBL international) in a total volume of 12 μl in 1× caspase activity buffer + 10 mM DTT. Samples were incubated at 37°C for 1 h to induce ATG16L1 cleavage, and then, the reaction was stopped by adding 2× sample loading buffer and boiled for 5 min.

Organoid culture

Colon organoids were established from Wt and $Ikk\alpha^{AA/AA}$ mice from a mixed background as previously described (Sato et al., 2009) and cultured as described for human colon cultures (Sato et al., 2011). In brief, colonic organoids were cultured in ENR medium (Advanced DMEM/F12 [Invitrogen], Hepes [Invitrogen], penicillin/streptomycin [Invitrogen], Glutamax [Invitrogen], 1× B27 [Invitrogen], 1× N2 [Invitrogen], 80 μM *N*-acetylcysteine [Sigma-Aldrich], 20% Noggin [in-house produced], 10% R-spondin [in-house produced], 200 ng/ml mouse epidermal growth factor, supplemented with 3.4 μg/ml Rock inhibitor [Sigma-Aldrich], 5 μM CHIR [Axon], 500 nM A83-01 [Tocris Bioscience], and 10 mM nicotinamide [Sigma-Aldrich]). The organoids were grown in Matrigel (BD) in 48-well plates and passaged at a 1:3 ratio once a week. The medium was changed every 2 d, and stimulations were performed in unsupplemented ENR medium, in the absence of *N*-acetylcysteine.

Isolation of IECs and lamina propria cells

After dissection, colons were excised and flashed with RPMI medium supplemented with penicillin and streptomycin (Invitrogen) and gentamycin (Invitrogen). Then, colons were cut in small pieces and incubated with gentle shaking for 30 min at 37°C in RPMI medium containing antibiotics, 5 mM EDTA (Roth), 3% FCS (Invitrogen), and 0.145 mg/ml DTT (Sigma-Aldrich). For IEC isolation, the supernatant was filtered with 100-μM strainers and centrifuged, and the pellet was resuspended in 30% (vol/vol) Percoll (GE Healthcare). The top layer was isolated, and 100,000 cells were plated on collagen type I (GE Healthcare)–precoated 96-well plates and cultured overnight. For isolation of lamina propria cells, the residual colon pieces were incubated in RPMI medium containing antibiotics, 0.1 mg/ml Liberase (Roche), and 0.05% DNase (Roche) for 30 min at 37°C with gentle shaking. Then, the supernatant was filtered with 70-μM strainers, and pelleted cells were washed two times in RPMI medium containing 10% FCS. Myeloid cells were sorted with a flow cytometer (FACS Aria; BD) using anti–Ly-6G (eBioscience), anti-CD45 (eBioscience), and anti-CD11b (eBioscience), seeded on 96-well plates, and cultured overnight. The remainder of the lamina propria cells (mostly lymphocytes) indicated as others were cultured as well along with the myeloid and IECs.

RNA analysis, *Xbp1* splicing, and densitometry quantification

Total RNA from intestinal mucosa, isolated epithelial cells, or colon organoids was extracted using an RNeasy Mini kit (QIAGEN). SuperScript II Reverse transcription (Invitrogen) was used for cDNA synthesis and real-time PCR analysis using FastStart Universal SYBR Master mix (Roche) in 20-μl total volume on a StepOne Plus Real-Time PCR system (Applied Biosystems). Relative gene expression levels were quantified by using cyclophilin as a housekeeping gene ($2^{[Ct\ cyclophilin\ -\ Ct\ target\ gene]}$). The PCR product of *Xbp1* unspliced (205 bp) and spliced (179 bp) were resolved on 2% agarose gel. Densitometric quantification of *Xbp1* splicing and immunoblots was performed with Adobe Photoshop.

ELISA and IL-18 treatment

Secreted IL-18 levels in blood sera were determined by the commercially available IL-18 ELISA kit according to the manufacturer's instructions (MBL international). For IL-18 rescue experiments, recombinant IL-18 (MBL international) dissolved in cold PBS (Invitrogen) was injected intraperitoneally at a concentration of 0.5 μg/mouse every day during the acute DSS treatment.

Bone marrow chimeras

Bone marrows were isolated from femur and tibia of $Ikk\alpha^{Wt/Wt}$ and $Ikk\alpha^{AA/AA}$ congenic donors. Recipient mice were irradiated with a lethal dose of 9 Gy to get rid of the immune cells and were injected with 4×10^6 cells in 100 μl PBS in the tail vein. The transplanted mice were given broad-

spectrum antibiotic (Ciprobay; Bayer) at a concentration of 1 mg/ml for 2 wk in drinking water. After 8 wk in total, the mice were treated with DSS and sacrificed on day 9. Colons were collected and stained for H&E.

Transmission electron microscopy

Transmission electron microscopy was used to visualize ultrastructural changes in mouse ileal tissue. Therefore, ileal tissues were initially fixed overnight using 2.5% glutaraldehyde buffered in cacodylate. The embedding procedure comprised fixation in 1% osmium tetroxide, dehydration in a graded ethanol series with an incubation step with uranyl acetate (between the 50 and 90% ethanol step), and finally rinsing in propylene oxide. The specimens were then embedded in epoxy resins that polymerized for 16 h at 60°C. After embedding, semithin sections (0.5 µm) were cut using an ultra-microtome (Ultracut UCT; Leica Biosystems) with a diamond knife. Sections were stained with Toluidine blue, placed on glass slides, and examined by light microscopy to select appropriate areas for ultrathin preparation. Ultrathin sections (50–70 nm) were cut again using an ultra-microtome. Sections were mounted on copper grids and contrasted with uranyl acetate for 2–3 h at 42°C followed by lead citrate for 20 min at room temperature. Imaging was performed using a transmission electron microscope (Tecnai G2 Spirit Biotwin; Thermo Fisher Scientific) at an operating voltage of 120 kV.

Mass spectrometry

Peptide fractions were analyzed on a quadrupole Orbitrap mass spectrometer (Q Exactive Plus; Thermo Fisher Scientific) equipped with an ultrahigh performance liquid chromatography system (EASY-nLC 1000; Thermo Fisher Scientific) as described previously (Cox et al., 2011). Peptide samples were loaded onto C18 reversed phase columns (15 cm length, 75 µm inner diameter, and 1.9 µm bead size) and eluted with a linear gradient from 8 to 40% acetonitrile containing 0.1% formic acid in 2 h. The mass spectrometer was operated in data-dependent mode, automatically switching between MS and MS2 acquisition. Survey full scan MS spectra (m/z 300–1700) were acquired in the Orbitrap. The 10 most intense ions were sequentially isolated and fragmented by higher-energy C-trap dissociation (Olsen et al., 2007). An ion selection threshold of 5,000 was used. Peptides with unassigned charge states, as well as with charge states <2 were excluded from fragmentation. Fragment spectra were acquired in the Orbitrap mass analyzer. Raw data files were analyzed using MaxQuant (version 1.5.2.8; Cox and Mann, 2008). Parent ion and MS2 spectra were searched against a database containing 88,473 human protein sequences obtained from the UniProtKB released in December 2013 using the Andromeda search engine (Cox et al., 2011). Spectra were searched with a mass tolerance of 6 ppm in MS mode, 20 ppm in higher-energy C-trap dissociation MS2 mode, strict trypsin specificity, and allowing up to three miscleavages. Cysteine carbamidomethylation was searched as a fixed modification, whereas protein N-terminal acetylation, methionine oxidation, and phosphorylation of serines, threonines, and tyrosines were variable modifications. Site localization probabilities were determined by MaxQuant using the posttranslational modification scoring algorithm as described previously (Olsen et al., 2006; Cox and Mann, 2008). The dataset was filtered based on posterior error probability to arrive at a false discovery rate of <1% estimated using a target-decoy approach.

Statistical analysis

Data are expressed as mean ± SE. Two-tailed Student's *t* test and ANOVA followed by Bonferroni posthoc test were performed for statistical analysis of two and multiple datasets, respectively, using Prism5 (GraphPad Software). P-values ≤ 0.05 were considered significant.

Online supplemental material

Fig. S1 shows that epithelial IKKα protects from DSS-induced colitis.

ACKNOWLEDGMENTS

We thank Natalia Delis, Kathleen Mohs, Christin Danneil, Eva Rudolf, and Petra Dinse for expert technical assistance.

This work was supported in part by the LOEWE Center for Cell and Gene Therapy Frankfurt (III L 4-518/17.004) and institutional funds from the Georg-Speyer-Haus, as well as grants from the Deutsche Forschungsgemeinschaft (SFB 1177 and Gr1916/11-1) and the European Research Council (ROSCAN- 281967) to F.R. Greten.

The authors declare no competing financial interests.

Author contributions: M.A. Diamanti, J. Gupta, M. Bennecke, T. De Oliveira, and M. Ramakrishnan performed and analyzed experiments. A.K. Braczynski and M. Mittelbronn conducted electron microscopy. B. Richter, P. Beli, and I. Dikic performed and analyzed mass spectrometry. Y. Hu and M. Saleh provided mouse strains. F.R. Greten designed the study. M.A. Diamanti, J. Gupta, and F.R. Greten wrote the manuscript.

Submitted: 4 November 2016
Revised: 29 November 2016
Accepted: 27 December 2016

REFERENCES

Abbott, D.W., A. Wilkins, J.M. Asara, and L.C. Cantley. 2004. The Crohn's disease protein, NOD2, requires RIP2 in order to induce ubiquitinylation of a novel site on NEMO. *Curr. Biol.* 14:2217–2227. http://dx.doi.org/10.1016/j.cub.2004.12.032

Adolph, T.E., M.F. Tomczak, L. Niederreiter, H.J. Ko, J. Böck, E. Martinez-Naves, J.N. Glickman, M. Tschurtschenthaler, J. Hartwig, S. Hosomi, et al. 2013. Paneth cells as a site of origin for intestinal inflammation. *Nature.* 503:272–276. http://dx.doi.org/10.1038/nature12599

Bollrath, J., and F.R. Greten. 2009. IKK/NF-κB and STAT3 pathways: central signalling hubs in inflammation-mediated tumour promotion and metastasis. *EMBO Rep.* 10:1314–1319. http://dx.doi.org/10.1038/embor.2009.243

Cadwell, K., J.Y. Liu, S.L. Brown, H. Miyoshi, J. Loh, J.K. Lennerz, C. Kishi, W. Kc, J.A. Carrero, S. Hunt, et al. 2008. A key role for autophagy and the autophagy gene Atg16l1 in mouse and human intestinal Paneth cells. *Nature.* 456:259–263. http://dx.doi.org/10.1038/nature07416

Calfon, M., H. Zeng, F. Urano, J.H. Till, S.R. Hubbard, H.P. Harding, S.G. Clark, and D. Ron. 2002. IRE1 couples endoplasmic reticulum load to secretory capacity by processing the XBP-1 mRNA. *Nature.* 415:92–96. http://dx.doi.org/10.1038/415092a

Cao, Y., G. Bonizzi, T.N. Seagroves, F.R. Greten, R. Johnson, E.V. Schmidt, and M. Karin. 2001. IKKα provides an essential link between RANK signaling and cyclin D1 expression during mammary gland development. *Cell*. 107:763–775. http://dx.doi.org/10.1016/S0092-8674(01)00599-2

Clausen, B.E., C. Burkhardt, W. Reith, R. Renkawitz, and I. Förster. 1999. Conditional gene targeting in macrophages and granulocytes using LysMcre mice. *Transgenic Res.* 8:265–277. http://dx.doi.org/10.1023/A:1008942828960

Comb, W.C., P. Cogswell, R. Sitcheran, and A.S. Baldwin. 2011. IKK-dependent, NF-κB-independent control of autophagic gene expression. *Oncogene*. 30:1727–1732. http://dx.doi.org/10.1038/onc.2010.553

Cox, J., and M. Mann. 2008. MaxQuant enables high peptide identification rates, individualized p.p.b.-range mass accuracies and proteome-wide protein quantification. *Nat. Biotechnol.* 26:1367–1372. http://dx.doi.org/10.1038/nbt.1511

Cox, J., N. Neuhauser, A. Michalski, R.A. Scheltema, J.V. Olsen, and M. Mann. 2011. Andromeda: a peptide search engine integrated into the MaxQuant environment. *J. Proteome Res.* 10:1794–1805. http://dx.doi.org/10.1021/pr101065j

Criollo, A., L. Senovilla, H. Authier, M.C. Maiuri, E. Morselli, I. Vitale, O. Kepp, E. Tasdemir, L. Galluzzi, S. Shen, et al. 2010. The IKK complex contributes to the induction of autophagy. *EMBO J.* 29:619–631. http://dx.doi.org/10.1038/emboj.2009.364

Djavaheri-Mergny, M., M. Amelotti, J. Mathieu, F. Besançon, C. Bauvy, S. Souquère, G. Pierron, and P. Codogno. 2006. NF-κB activation represses tumor necrosis factor-α-induced autophagy. *J. Biol. Chem.* 281:30373–30382. http://dx.doi.org/10.1074/jbc.M602097200

Dupaul-Chicoine, J., G. Yeretssian, K. Doiron, K.S. Bergstrom, C.R. McIntire, P.M. LeBlanc, C. Meunier, C. Turbide, P. Gros, N. Beauchemin, et al. 2010. Control of intestinal homeostasis, colitis, and colitis-associated colorectal cancer by the inflammatory caspases. *Immunity.* 32:367–378. http://dx.doi.org/10.1016/j.immuni.2010.02.012

Eckmann, L., T. Nebelsiek, A.A. Fingerle, S.M. Dann, J. Mages, R. Lang, S. Robine, M.F. Kagnoff, R.M. Schmid, M. Karin, et al. 2008. Opposing functions of IKKβ during acute and chronic intestinal inflammation. *Proc. Natl. Acad. Sci. USA.* 105:15058–15063. http://dx.doi.org/10.1073/pnas.0808216105

Elinav, E., T. Strowig, A.L. Kau, J. Henao-Mejia, C.A. Thaiss, C.J. Booth, D.R. Peaper, J. Bertin, S.C. Eisenbarth, J.I. Gordon, and R.A. Flavell. 2011. NLRP6 inflammasome regulates colonic microbial ecology and risk for colitis. *Cell*. 145:745–757. http://dx.doi.org/10.1016/j.cell.2011.04.022

Fabre, C., G. Carvalho, E. Tasdemir, T. Braun, L. Adès, J. Grosjean, S. Boehrer, D. Métivier, S. Souquère, G. Pierron, et al. 2007. NF-κB inhibition sensitizes to starvation-induced cell death in high-risk myelodysplastic syndrome and acute myeloid leukemia. *Oncogene.* 26:4071–4083. http://dx.doi.org/10.1038/sj.onc.1210187

Giacomin, P.R., R.H. Moy, M. Noti, L.C. Osborne, M.C. Siracusa, T. Alenghat, B. Liu, K.A. McCorkell, A.E. Troy, G.D. Rak, et al. 2015. Epithelial-intrinsic IKKα expression regulates group 3 innate lymphoid cell responses and antibacterial immunity. *J. Exp. Med.* 212:1513–1528. http://dx.doi.org/10.1084/jem.20141831

Greten, F.R., L. Eckmann, T.F. Greten, J.M. Park, Z.W. Li, L.J. Egan, M.F. Kagnoff, and M. Karin. 2004. IKKβ links inflammation and tumorigenesis in a mouse model of colitis-associated cancer. *Cell*. 118:285–296. http://dx.doi.org/10.1016/j.cell.2004.07.013

Häcker, H., and M. Karin. 2006. Regulation and function of IKK and IKK-related kinases. *Sci. STKE.* 2006:re13. http://dx.doi.org/10.1126/stke.3572006re13

Hampe, J., A. Franke, P. Rosenstiel, A. Till, M. Teuber, K. Huse, M. Albrecht, G. Mayr, F.M. De La Vega, J. Briggs, et al. 2007. A genome-wide association scan of nonsynonymous SNPs identifies a susceptibility variant for Crohn disease in ATG16L1. *Nat. Genet.* 39:207–211. http://dx.doi.org/10.1038/ng1954

Homer, C.R., A.L. Richmond, N.A. Rebert, J.P. Achkar, and C. McDonald. 2010. ATG16L1 and NOD2 interact in an autophagy-dependent antibacterial pathway implicated in Crohn's disease pathogenesis. *Gastroenterology.* 139:1630–1641.e2. http://dx.doi.org/10.1053/j.gastro.2010.07.006

Hotamisligil, G.S. 2010. Endoplasmic reticulum stress and the inflammatory basis of metabolic disease. *Cell*. 140:900–917. http://dx.doi.org/10.1016/j.cell.2010.02.034

Hu, P., Z. Han, A.D. Couvillon, R.J. Kaufman, and J.H. Exton. 2006. Autocrine tumor necrosis factor alpha links endoplasmic reticulum stress to the membrane death receptor pathway through IRE1α-mediated NF-κB activation and down-regulation of TRAF2 expression. *Mol. Cell. Biol.* 26:3071–3084. http://dx.doi.org/10.1128/MCB.26.8.3071-3084.2006

Hugot, J.P., M. Chamaillard, H. Zouali, S. Lesage, J.P. Cézard, J. Belaiche, S. Almer, C. Tysk, C.A. O'Morain, M. Gassull, et al. 2001. Association of NOD2 leucine-rich repeat variants with susceptibility to Crohn's disease. *Nature.* 411:599–603. http://dx.doi.org/10.1038/35079107

Kaser, A., A.H. Lee, A. Franke, J.N. Glickman, S. Zeissig, H. Tilg, E.E. Nieuwenhuis, D.E. Higgins, S. Schreiber, L.H. Glimcher, and R.S. Blumberg. 2008. XBP1 links ER stress to intestinal inflammation and confers genetic risk for human inflammatory bowel disease. *Cell*. 134:743–756. http://dx.doi.org/10.1016/j.cell.2008.07.021

Kitajima, S., S. Takuma, and M. Morimoto. 1999. Changes in colonic mucosal permeability in mouse colitis induced with dextran sulfate sodium. *Exp. Anim.* 48:137–143. http://dx.doi.org/10.1538/expanim.48.137

Kwak, Y.T., J. Guo, J. Shen, and R.B. Gaynor. 2000. Analysis of domains in the IKKα and IKKβ proteins that regulate their kinase activity. *J. Biol. Chem.* 275:14752–14759. http://dx.doi.org/10.1074/jbc.M001039200

Lassen, K.G., P. Kuballa, K.L. Conway, K.K. Patel, C.E. Becker, J.M. Peloquin, E.J. Villablanca, J.M. Norman, T.C. Liu, R.J. Heath, et al. 2014. Atg16L1 T300A variant decreases selective autophagy resulting in altered cytokine signaling and decreased antibacterial defense. *Proc. Natl. Acad. Sci. USA.* 111:7741–7746. http://dx.doi.org/10.1073/pnas.1407001111

Li, N., X. Wu, R.G. Holzer, J.H. Lee, J. Todoric, E.J. Park, H. Ogata, A.S. Gukovskaya, I. Gukovsky, D.P. Pizzo, et al. 2013. Loss of acinar cell IKKα triggers spontaneous pancreatitis in mice. *J. Clin. Invest.* 123:2231–2243. http://dx.doi.org/10.1172/JCI64498

Madison, B.B., L. Dunbar, X.T. Qiao, K. Braunstein, E. Braunstein, and D.L. Gumucio. 2002. Cis elements of the villin gene control expression in restricted domains of the vertical (crypt) and horizontal (duodenum, cecum) axes of the intestine. *J. Biol. Chem.* 277:33275–33283. http://dx.doi.org/10.1074/jbc.M204935200

Muñoz, M., C. Eidenschenk, N. Ota, K. Wong, U. Lohmann, A.A. Kühl, X. Wang, P. Manzanillo, Y. Li, S. Rutz, et al. 2015. Interleukin-22 induces interleukin-18 expression from epithelial cells during intestinal infection. *Immunity.* 42:321–331. http://dx.doi.org/10.1016/j.immuni.2015.01.011

Murthy, A., Y. Li, I. Peng, M. Reichelt, A.K. Katakam, R. Noubade, M. Roose-Girma, J. DeVoss, L. Diehl, R.R. Graham, and M. van Lookeren Campagne. 2014. A Crohn's disease variant in Atg16l1 enhances its degradation by caspase 3. *Nature.* 506:456–462. http://dx.doi.org/10.1038/nature13044

Nenci, A., C. Becker, A. Wullaert, R. Gareus, G. van Loo, S. Danese, M. Huth, A. Nikolaev, C. Neufert, B. Madison, et al. 2007. Epithelial NEMO links innate immunity to chronic intestinal inflammation. *Nature.* 446:557–561. http://dx.doi.org/10.1038/nature05698

Neurath, M.F., S. Pettersson, K.H. Meyer zum Büschenfelde, and W. Strober. 1996. Local administration of antisense phosphorothioate oligonucleotides to the p65 subunit of NF-κB abrogates established experimental colitis in mice. *Nat. Med.* 2:998–1004. http://dx.doi.org/10.1038/nm0996-998

Nivon, M., E. Richet, P. Codogno, A.P. Arrigo, and C. Kretz-Remy. 2009. Autophagy activation by NFκB is essential for cell survival after heat shock. *Autophagy.* 5:766–783. http://dx.doi.org/10.4161/auto.8788

Ogura, Y., D.K. Bonen, N. Inohara, D.L. Nicolae, F.F. Chen, R. Ramos, H. Britton, T. Moran, R. Karaliuskas, R.H. Duerr, et al. 2001. A frameshift mutation in NOD2 associated with susceptibility to Crohn's disease. *Nature.* 411:603–606. http://dx.doi.org/10.1038/35079114

Olsen, J.V., B. Blagoev, F. Gnad, B. Macek, C. Kumar, P. Mortensen, and M. Mann. 2006. Global, in vivo, and site-specific phosphorylation dynamics in signaling networks. *Cell.* 127:635–648. http://dx.doi.org/10.1016/j.cell.2006.09.026

Olsen, J.V., B. Macek, O. Lange, A. Makarov, S. Horning, and M. Mann. 2007. Higher-energy C-trap dissociation for peptide modification analysis. *Nat. Methods.* 4:709–712. http://dx.doi.org/10.1038/nmeth1060

Paxian, S., H. Merkle, M. Riemann, M. Wilda, G. Adler, H. Hameister, S. Liptay, K. Pfeffer, and R.M. Schmid. 2002. Abnormal organogenesis of Peyer's patches in mice deficient for NF-κB1, NF-κB2, and Bcl-3. *Gastroenterology.* 122:1853–1868. http://dx.doi.org/10.1053/gast.2002.33651

Qing, G., P. Yan, Z. Qu, H. Liu, and G. Xiao. 2007. Hsp90 regulates processing of NF-κ B2 p100 involving protection of NF-κB-inducing kinase (NIK) from autophagy-mediated degradation. *Cell Res.* 17:520–530. http://dx.doi.org/10.1038/cr.2007.47

Rioux, J.D., R.J. Xavier, K.D. Taylor, M.S. Silverberg, P. Goyette, A. Huett, T. Green, P. Kuballa, M.M. Barmada, L.W. Datta, et al. 2007. Genome-wide association study identifies new susceptibility loci for Crohn disease and implicates autophagy in disease pathogenesis. *Nat. Genet.* 39:596–604. http://dx.doi.org/10.1038/ng2032

Saleh, M., J.C. Mathison, M.K. Wolinski, S.J. Bensinger, P. Fitzgerald, N. Droin, R.J. Ulevitch, D.R. Green, and D.W. Nicholson. 2006. Enhanced bacterial clearance and sepsis resistance in caspase-12-deficient mice. *Nature.* 440:1064–1068. http://dx.doi.org/10.1038/nature04656

Sato, T., R.G. Vries, H.J. Snippert, M. van de Wetering, N. Barker, D.E. Stange, J.H. van Es, A. Abo, P. Kujala, P.J. Peters, and H. Clevers. 2009. Single Lgr5 stem cells build crypt-villus structures in vitro without a mesenchymal niche. *Nature.* 459:262–265. http://dx.doi.org/10.1038/nature07935

Sato, T., D.E. Stange, M. Ferrante, R.G. Vries, J.H. Van Es, S. Van den Brink, W.J. Van Houdt, A. Pronk, J. Van Gorp, P.D. Siersema, and H. Clevers. 2011. Long-term expansion of epithelial organoids from human colon, adenoma, adenocarcinoma, and Barrett's epithelium. *Gastroenterology.* 141:1762–1772. http://dx.doi.org/10.1053/j.gastro.2011.07.050

Schirbel, A., and C. Fiocchi. 2010. Inflammatory bowel disease: Established and evolving considerations on its etiopathogenesis and therapy. *J. Dig. Dis.* 11:266–276. http://dx.doi.org/10.1111/j.1751-2980.2010.00449.x

Schroder, K., and J. Tschopp. 2010. The inflammasomes. *Cell.* 140:821–832. http://dx.doi.org/10.1016/j.cell.2010.01.040

Senftleben, U., Y. Cao, G. Xiao, F.R. Greten, G. Krähn, G. Bonizzi, Y. Chen, Y. Hu, A. Fong, S.C. Sun, and M. Karin. 2001. Activation by IKKα of a second, evolutionary conserved, NF-κB signaling pathway. *Science.* 293:1495–1499. http://dx.doi.org/10.1126/science.1062677

Sorbara, M.T., L.K. Ellison, M. Ramjeet, L.H. Travassos, N.L. Jones, S.E. Girardin, and D.J. Philpott. 2013. The protein ATG16L1 suppresses inflammatory cytokines induced by the intracellular sensors Nod1 and Nod2 in an autophagy-independent manner. *Immunity.* 39:858–873. http://dx.doi.org/10.1016/j.immuni.2013.10.013

Takagi, H., T. Kanai, A. Okazawa, Y. Kishi, T. Sato, H. Takaishi, N. Inoue, H. Ogata, Y. Iwao, K. Hoshino, et al. 2003. Contrasting action of IL-12 and IL-18 in the development of dextran sodium sulphate colitis in mice. *Scand. J. Gastroenterol.* 38:837–844. http://dx.doi.org/10.1080/00365520310004047

Takeda, K., O. Takeuchi, T. Tsujimura, S. Itami, O. Adachi, T. Kawai, H. Sanjo, K. Yoshikawa, N. Terada, and S. Akira. 1999. Limb and skin abnormalities in mice lacking IKKα. *Science.* 284:313–316. http://dx.doi.org/10.1126/science.284.5412.313

Travassos, L.H., L.A. Carneiro, M. Ramjeet, S. Hussey, Y.G. Kim, J.G. Magalhães, L. Yuan, F. Soares, E. Chea, L. Le Bourhis, et al. 2010. Nod1 and Nod2 direct autophagy by recruiting ATG16L1 to the plasma membrane at the site of bacterial entry. *Nat. Immunol.* 11:55–62. http://dx.doi.org/10.1038/ni.1823

Wehkamp, J., J. Harder, M. Weichenthal, M. Schwab, E. Schäffeler, M. Schlee, K.R. Herrlinger, A. Stallmach, F. Noack, P. Fritz, et al. 2004. NOD2 (CARD15) mutations in Crohn's disease are associated with diminished mucosal α-defensin expression. *Gut.* 53:1658–1664. http://dx.doi.org/10.1136/gut.2003.032805

Yoneda, T., K. Imaizumi, K. Oono, D. Yui, F. Gomi, T. Katayama, and M. Tohyama. 2001. Activation of caspase-12, an endoplastic reticulum (ER) resident caspase, through tumor necrosis factor receptor-associated factor 2-dependent mechanism in response to the ER stress. *J. Biol. Chem.* 276:13935–13940.

Zaki, M.H., K.L. Boyd, P. Vogel, M.B. Kastan, M. Lamkanfi, and T.D. Kanneganti. 2010. The NLRP3 inflammasome protects against loss of epithelial integrity and mortality during experimental colitis. *Immunity.* 32:379–391. http://dx.doi.org/10.1016/j.immuni.2010.03.003

Zaph, C., A.E. Troy, B.C. Taylor, L.D. Berman-Booty, K.J. Guild, Y. Du, E.A. Yost, A.D. Gruber, M.J. May, F.R. Greten, et al. 2007. Epithelial-cell-intrinsic IKK-β expression regulates intestinal immune homeostasis. *Nature.* 446:552–556. http://dx.doi.org/10.1038/nature05590